ACS Catalysis

Research Article

pubs.acs.org/acscatalysis

Ring Contraction Catalyzed by the Metal-Dependent Radical SAM Enzyme: 7-Carboxy-7-deazaguanine Synthase from *B. multivorans*. Theoretical Insights into the Reaction Mechanism and the Influence of Metal Ions

Wenyou Zhu[†] and Yongjun Liu*[,†,‡]

[†]Key Laboratory of Colloid and Interface Chemistry, Ministry of Education, School of Chemistry and Chemical Engineering, Shandong University, Jinan, Shandong 250100, China

[‡]Key Laboratory of Tibetan Medicine Research, Northwest Institute of Plateau Biology, Chinese Academy of Sciences, Xining, Qinghai 810001, China

Supporting Information

ABSTRACT: 7-Carboxy-7-deazaguanine synthase (QueE) is a radical *S*-adenosylmethionine (SAM) enzyme that catalyzes the conversion of 6-carboxy-5,6,7,8-tetrahydropterin (CPH_4) to 7-carboxy-7-deazaguanine (CDG). QueE also shows a clear dependence on Mg^{2+} ion and is considered a new feature for a radical SAM enzyme. The catalytic mechanism of QueE from *B. multivorans* has been studied using a combined quantum mechanics and molecular mechanics (QM/MM) method. The results of our calculations reveal that the key ring-contraction step involves a bridged intermediate rather than a ring-opening one. For the QueE−Mg^{2+} system, the elimination of ammonia is calculated to be rate limiting with a free energy barrier of 18.8 kcal/mol, which is basically in accordance with the estimated value (20.9 kcal/mol) from the experiment. For QueE−Na^+ complex, the rate-limiting step switches to the formation of the bridged intermediate with an energy barrier of 29.3 kcal/mol. Natural population analysis indicates that the metal ions do not act as Lewis acids; therefore, they mainly play a role in fixing the substrate in its reactive conformation. The different coordination of Mg^{2+} and Na^+ with the substrate is suggested to be the main reason for leading to the different activities of QueE−Mg^{2+} and QueE−Na^+ complexes.

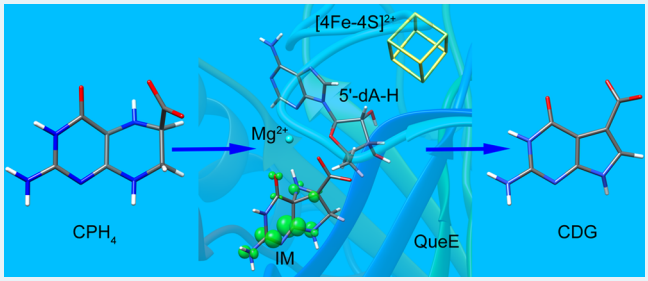

KEYWORDS: *7-carboxy-7-deazaguanine synthase (QueE), reaction mechanism, 7-carboxy-7-deazaguanine (CDG), 6-carboxy-5,6,7,8-tetrahydropterin (CPH_4), QM/MM, SAM radical enzyme*

1. INTRODUCTION

Pyrrolopyrimidine-containing compounds, also called 7-deazapurines, are widely distributed in nature and include a series of structurally diverse nucleoside analogues that exhibit antineoplastic and antibiotic activities.[1−4] 7-Deazapurine moieties are also found in the hypermodified *t*RNA nucleosides queuosine and archaeosine.[5,6] Queuosine was found to occupy the first anticodon position of *t*RNAs for histidine, aspartic acid, asparagine, and tyrosine.[7−9] The precise physiological role of the hypermodification remains uncharacterized. Archaeosine is located at the dihydrouridine loop of most archaeal *t*RNAs and has the function to stabilize the tertiary RNAs structures.[6,10]

On the basis of the previous studies, the 7-deazapurine moiety, which is the core of pyrrolopyrimidine nucleosides, can be biosynthesized via a series of common pathways from guanosine 5′-triphosphate (GTP) involving four enzymes, GTP cyclohydrolase I (GCHI), 7-cyano-7-deazaguanine ($preQ_0$) synthase (QueC), 6-carboxy-5,6,7,8-tetrahydropterin (CPH_4) synthase (QueD), and 7-carboxy-7-deazaguanine (CDG) synthase (QueE), as shown in Scheme 1.[4,11,12] GTP is first converted by GCHI and QueD to CPH_4.[13−15] Then CPH_4 is transformed by QueE to CDG,[11] which is further converted to the central $preQ_0$ intermediate. From CPH_4 to CDG, a complex and unprecedented heterocyclic rearrangement is involved, and CDG is thought to be a central precursor for all 7-deazapurine-containing compounds.[12]

CDG synthase (QueE) belongs to the radical S-adenosylmethionine (SAM) enzyme superfamily, which was first classified in 2001.[4,12,16,17] A typical feature of the radical SAM enzymes is the presence of a $CX_3CX\Phi C$ motif, which is conserved in almost all known radical SAM enzymes. The three cysteine residues of $CX_3CX\Phi C$ motif coordinate with three of the iron atoms of the essential [4Fe−4S] cluster in the active site.[18−22] The remaining fourth iron atom binds with both the α-amino

Received: January 25, 2015
Revised: May 18, 2015
Published: May 21, 2015

DOI: 10.1021/acscatal.5b00156
ACS Catal. 2015, 5, 3953−3965

Scheme 1. Biosynthesis Pathway of CDG[4,11,12]

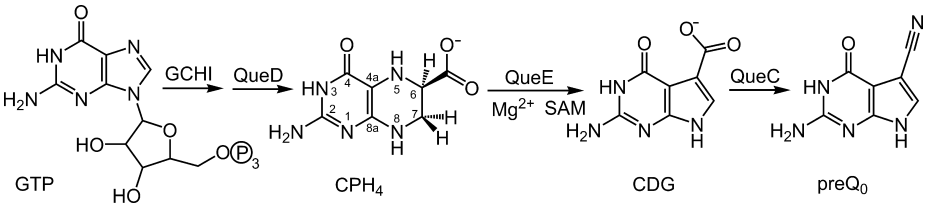

Scheme 2. Reductive Cleavage of the S−C5′ Bond of SAM[21]

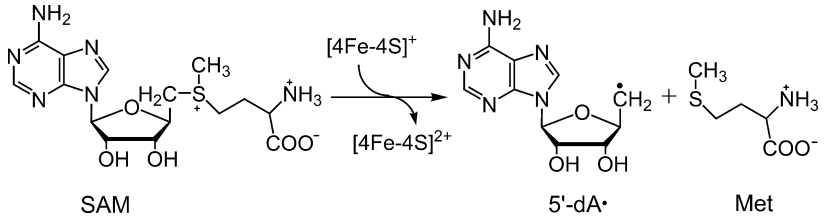

and α-carboxylate groups of SAM, forming a five-membered chelate ring.[23−26] During the catalytic reactions, one electron transfers from the +1 oxidation state of the [4Fe−4S] cluster to SAM, leading to the reductive cleavage of the S−C5′ bond and the formation of a methionine and a highly reactive 5′-deoxyadenosyl radical (5′-dA$^{\bullet}$) (Scheme 2). This radical (5′-dA$^{\bullet}$) can abstract a hydrogen atom from either the substrate molecule or other residue of the protein to initiate a variety of enzymatic reactions, including DNA repair, enzyme activation, protein and nucleic acid modification, primary metabolism, and cofactor synthesis.[27,28]

Although QueE belongs to the SAM superfamily, it exhibits a clear structural difference compared to the common SAM enzyme. Most of the SAM radical enzymes obtained so far display the adoption of either a partial or full $(\beta/\alpha)_8$ triose−phosphate isomerase (TIM) barrel fold,[18−22,29] which is called the SAM radical core. Whereas QueE from *B. multivorans* adopts both a noncanonical cluster-binding $CX_{14}CX\Phi C$ motif and a hypermodified protein fold named ($\beta6/\alpha3$) architecture,[29] where a short 3_{10}-helix (3_{10}H5) and two short loops (*L*3 and *L*4) replace the three α-helices ($\alpha3$, $\alpha4$, and $\alpha5$) of the common SAM radical fold. In addition, QueE also shows a metal dependence.[29,30] For example, in the assays of QueE from *B. multivorans*, Mg^{2+} enhances the activity by 3-fold, but Na^{+} and Mn^{2+} do not accelerate the QueE activity. It should be noted that the QueE from *B. subtilis* exhibits a different dependence of Mg^{2+}; i.e., Mg^{2+} can enhance the activity by approximately 10-fold. However, the crystal structure of QueE from *B. subtilis* has not determined yet.

As for the reaction mechanism of conversion of CPH_4 to CDG, several studies, including the spectroscopic and steady-state kinetic experiments, have been carried out to explore the biosynthetic pathway of CDG catalyzed by QueE from *B. subtilis*.[29,30] They demonstrated that QueE is indeed a member of the radial SAM superfamily. The isotope-transfer experiments afforded a clear evidence of the direct abstraction of a hydrogen atom from the C-6 of the substrate (CPH_4) by 5′-dA$^{\bullet}$ to initiate the complex chemical transformation. On the basis of their experimental observations, a working model that is consistent with the biochemical and spectroscopic data for the conversion of CPH_4 to CDG was proposed,[29,30] which is shown in Scheme 3. From the proposed mechanism, we have no idea how the ring rearrangement occurs. As shown in Scheme 3, the reaction may undergo either a hemolytic cleavage of the C4a−N5 bond of the substrate leading to the generation of an imine intermediate or formation of a C4a−C6 bond yielding a bridged azacyclopropylcarbinyl intermediate. Both of the routes have precedents to go by. The former resembles the Baldwin *5-exo-trig* radical-mediated ring closure,[31] while the latter is analogous to the central radical intermediate in the reaction catalyzed by lysine 2,3-aminomutase.[32]

In 2014, the crystal structures of QueE from *B. multivorans* were successfully determined in which all of the cofactors were reported, including the intact substrate and the product.[29] It was the best structurally characterized SAM radical enzyme. As described above, QueE is not only a SAM-dependent enzyme but also requires a metal ion (Mg^{2+}) for its catalysis.[29,30] As shown in Figure 1a, Mg^{2+} directly interacts with three water molecules, the hydroxyl group of Thr51 and the carboxyl and carbonyl groups of the substrate, forming a pseudo-octahedral structure. Mg^{2+} is supposed to play multiple important roles in the complex chemical transformation. QueE is the first member of the radical SAM superfamily that requires a divalent magnesium ion to assist its catalytic reaction. Bandarian and co-workers have proposed that Mg^{2+} may activate the C6 proton and thereby facilitate the hydrogen abstraction step by its interaction with the carboxyl and carbonyl groups of the substrate and acts as a Lewis acid to accelerate the ammonia molecule elimination.[30] It should be noted that these roles of Mg^{2+} are only based on the hypothesis. In addition, a monovalent Na^{+} ion can also stabilize the substrate in the active site by a similar coordination with the carboxyl group (Figure 1b), but the acceleration for activity was not observed.

QueE utilizes a 5′-dA radical and Mg^{2+} to catalyze the conversion of CPH_4 to CDG. As described above, several questions for the reaction details have no clear answers yet. For example, we still do not know how the key carbon skeleton rearrangement occurs, how the ammonia molecule eliminates, and how the five-membered ring aromatizes. To answer these questions, in this work, the combined quantum mechanics and molecular mechanics (QM/MM) method[33,34] has been employed to explore the catalytic mechanism of QueE from *B. multivorans*. The QM/MM method has been widely applied in elucidating the catalytic mechanism of extended systems,[35−39] including the radical SAM enzyme.[40−42] On the

DOI: 10.1021/acscatal.5b00156
ACS Catal. 2015, 5, 3953−3965

Scheme 3. Proposed Mechanism for QueE[29,30]

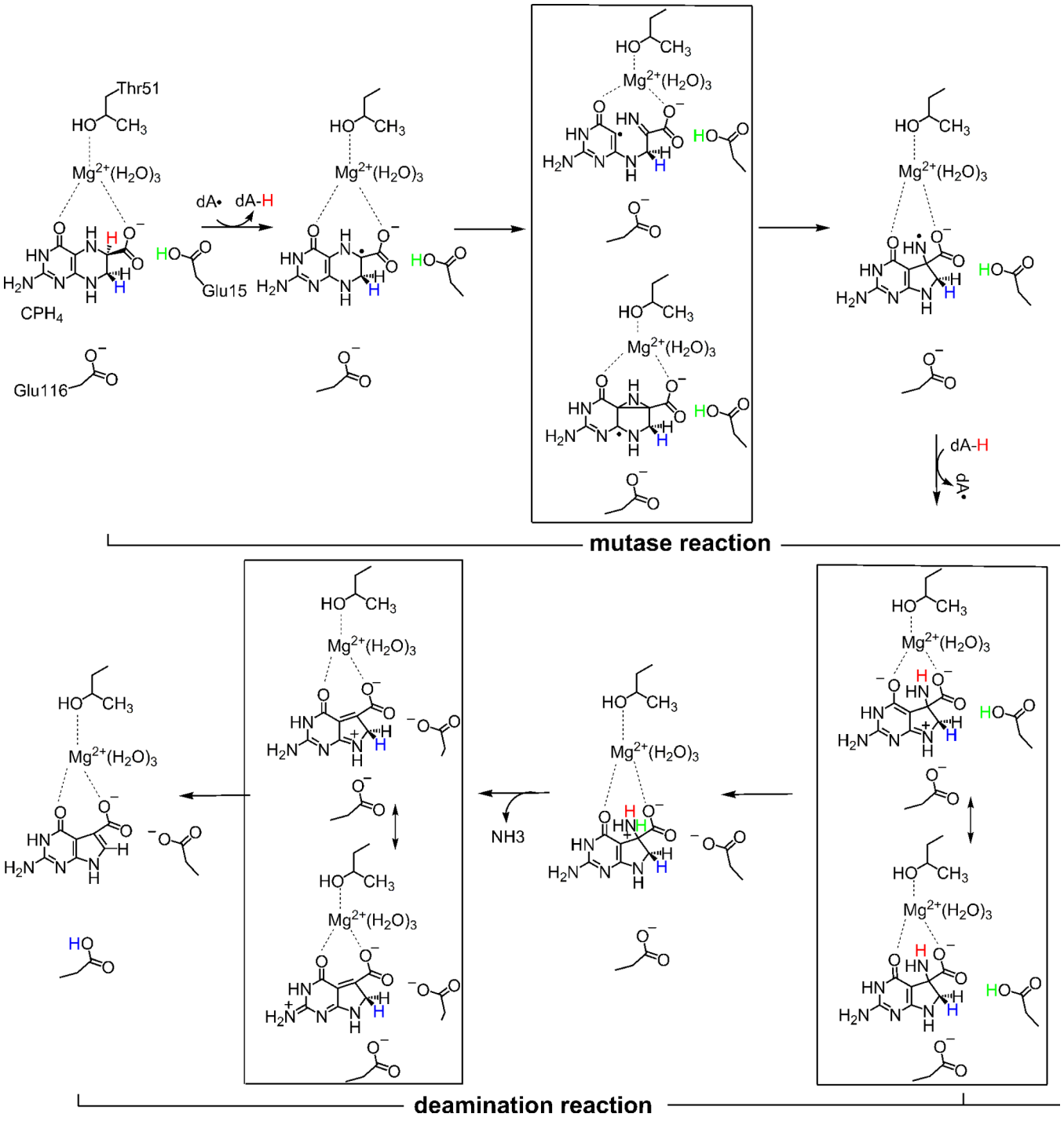

basis of the recently obtained crystal structures of QueE from *B. multivorans*, the reaction detail was illuminated, and the different influences of Mg^{2+} and Na^{+} on the reaction were compared as well.

2. METHODS

2.1. Computational Models. The crystal structures of QueE in complex with the [4Fe−4S] cluster, SAM, substrate, and Mg^{2+} or Na^{+} (PDB codes: 4NJI and 4NJH)[29] provided good templates for our theoretical studies. Both structural and biochemical analysis indicate that QueE is a homodimer with two identical monomers, and two identical active sites locate at the two monomers, respectively. Therefore, all of the atoms labeled "A" (chain A) in the pdb data were selected to construct the initial computational models. Based on the crystal structures of QueE in complex with Mg^{2+} and Na^{+}, two models were constructed. During the catalytic reaction, a proton abstraction process by the N5 atom of the NH_2 group of the initial product is required to facilitate the elimination of the ammonia molecule. By checking the crystal structures of QueE, we found that only residue Glu15 locates at a reasonable position to donate its proton to the NH_2 group. Thus, Glu15 was set to be protonated in the computational models. The protonation states of other titratable residues were assigned according to their pK_a values predicated by the PROPKA3.1 program[43−46] under the experimental conditions. Subsequently, the missing H atoms were put into the systems by

DOI: 10.1021/acscatal.5b00156
ACS Catal. 2015, 5, 3953−3965

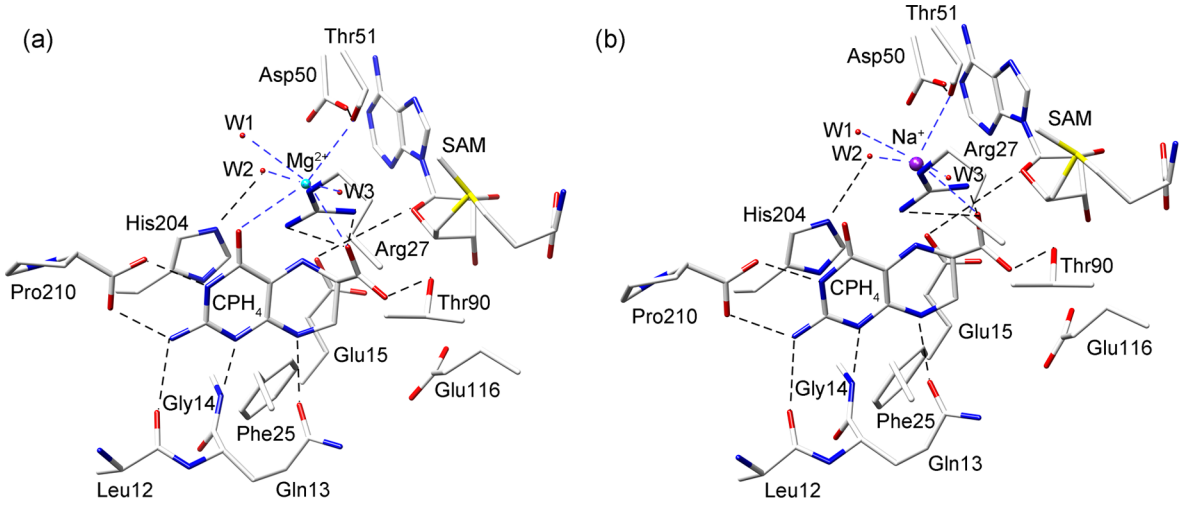

Figure 1. Crystal structures of active sites of QueE in complex with Mg^{2+} (a) and Na^{+} (b). The coordination bonds are shown in blue dashed lines and hydrogen bonds in black dashed lines.

using the HBUILD program in the CHARMM package.[47] Afterward, both of the systems were fully placed into the TIP3P[48] water spheres with a radius of 32 Å. The water molecules that located at less than 2.5 Å from the non-hydrogen atoms were deleted. To neutralize the systems, 8 or 9 Na^{+} were added into the QueE−Mg^{2+} or −Na^{+} complex at random positions, respectively. After a series of minimization steps, 20 ns MD simulations were performed to equilibrate the systems by using the CHARMM22/CMAP force field.[47,49,50] The prepared models were divided into an inner reaction region (r < 28 Å) and an outer buffer region (28 Å < r < 32 Å) during MD simulations, which were, respectively, described by Newton's equations of motion and Langevin dynamics with friction and random force. The MD simulations were performed by three steps: (1) the systems were first heated from 0 to 298.15 K for 50 ps with a time step of 1 fs; (2) the systems were then equilibrated for 50 ps at the 298.15 K with a time step of 1 fs; (3) and finally, 20 ns MD simulations were carried out. The Mg^{2+} and Na^{+} were frozen on their initial positions during the simulations.

2.2. QM/MM Calculations. In this work, the last snapshots taken from MD simulations were used as the reactant structures to perform the subsequent QM/MM calculations. Each system was divided into two regions: the QM region that was treated by DFT with B3LYP functional[51,52] in Turbomole[53] and the MM region that was characterized by the CHARMM22 force field[50] in DL-POLY.[54] Turbomole and DL-POLY programs were combined by the ChemShell package[55] in all QM/MM calculations. For a better description of the catalytic mechanism of QueE, the entire reaction was divided into two parts: the mutase and deamination reactions, as shown in Scheme 3. In the mutase process, the substrate CPH_4, 5′-dA radical, side chains of Glu15, Asp50, Glu116, and Pro210, part of the residue Ile209, Mg^{2+}, three Mg^{2+}-coordinated water molecules, and one coordinated residue Thr51 were included in the QM region, which is shown in Scheme 4. After MD simulations, a noncrystal water molecule was found to locate between the CPH_4 and Glu116. This water molecule may play an assistant role in the catalytic reaction. Therefore, it was also included in the QM region. Thus, the QM region totally contains 124 atoms. In the later stage of the deamination reaction, an ammonia molecule was formed, which was subsequently removed from the QM region. To investigate the dependence of metal ions, the mutase and deamination reactions catalyzed by the Na^{+}-containing QueE were also considered. The remaining atoms of systems were included in the MM regions.

Scheme 4. QM Region of Mutase Reaction[a]

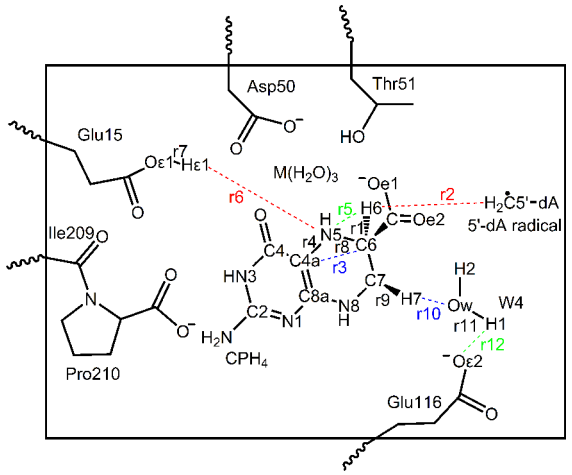

[a]In the calculation of the deamination reaction, an ammonia molecule was formed and then removed from the QM region. Atoms and distances mentioned in the text are labeled. M represents the Mg^{2+} or Na^{+}.

In this work, hydrogen link atoms were used to treat the QM/MM boundary with the charge shift model.[56] In addition, the polarizing effects of surrounding on the QM subsystem were accounted for by using an electronic embedding scheme[57] in which the MM region charges were incorporated into the one-electron Hamiltonian of the QM calculations. All structures along the reaction path were optimized at the basis set of 6-31G(d,p). The hybrid delocalized internal coordinates (HDLC) optimizer[58] was applied to perform the geometry optimizations, and the local minima were searched by using the quasi-Newton limited memory Broyden−Fletcher−Goldfarb−Shanno (L-BFGS) method.[59,60] The partitioned rational function optimization (P-RFO) algorithm[61] was used to find transition states by following eigenmodes of the Hessian. All obtained transition states were confirmed by only one single negative eigenvalue. On the basis of on the optimized structures, the single-point energies were calculated with the 6-311++G(3df,3pd) basis set, and the frequencies were performed at the 6-31G(d,p) level to calculate the entropy effect. As we all know, the dispersion interaction could not be accurately characterized by the B3LYP functional. Thus, the DFT-D3 program[62] was employed to correct the energies of dispersion. It should be noted that the correction of dispersion energies only applied for the QM regions, and the structures of QM regions were cut from the QM/

DOI: 10.1021/acscatal.5b00156
ACS Catal. 2015, 5, 3953−3965

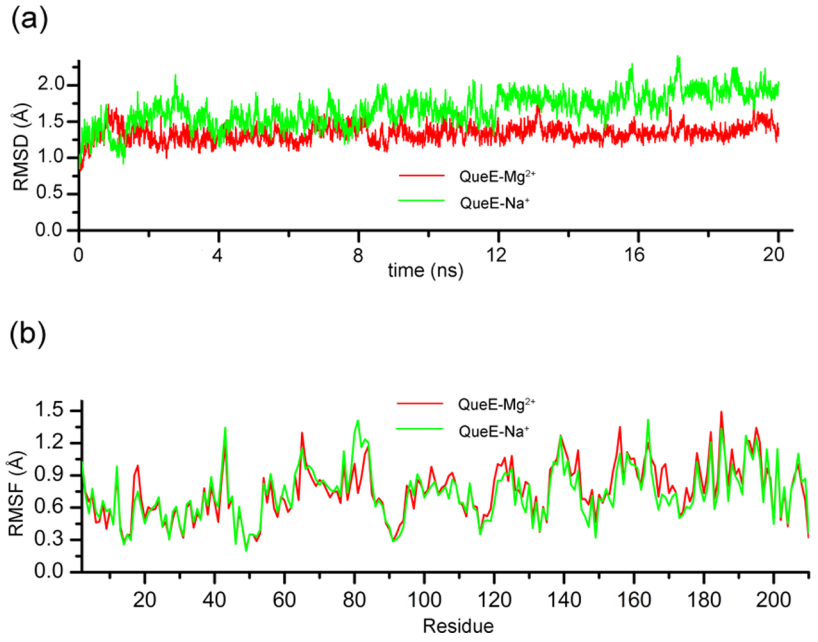

Figure 2. RMSDs and RMSFs of QueE in complex with Mg^{2+} and Na^{+} obtained from 20 ns MD simulations.

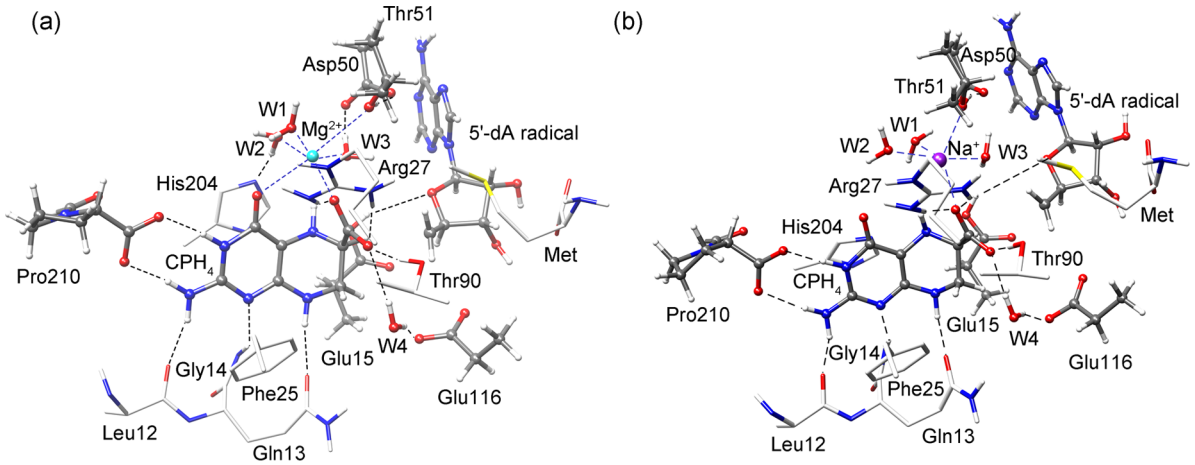

Figure 3. Optimized structures of active sites of QueE in complex with Mg^{2+} (a) and Na^{+} (b). The atoms in QM region are displayed in ball and stick models. Coordination bonds are shown in blue dashed lines and hydrogen bonds in black dashed lines.

MM-optimized geometries. The entropy contributions and empirical dispersion corrections are shown in Table S1. As shown in Table S1, both of the entropies and dispersion effects are minor. Besides, the natural population atomic charges of QM regions were calculated at the 6-31++G(d,p) level by using QM/MM methods, and the spin densities were calculated by using the Gaussian03 package[63] at the same level. During the QM/MM calculations, the MM region residues beyond 13 Å of the CPH_4 molecule were frozen, while the rest of the MM atoms were allowed to move. In addition, the potential energy surface (PES) was calculated at the B3LYP/6-31G(d,p) level to indicate how the key carbon skeleton rearrangement occurs.

3. RESULTS AND DISCUSSION

3.1. Structures of QueE in Complex with Mg^{2+} and Na^{+}. The crystal structures of QueE in complex with Mg^{2+} and Na^{+} were taken and subjected to a 20 ns MD simulations. The obtained root mean square deviations (RMSDs) and root mean square fluctuations (RMSFs) are displayed in Figure 2. One can see from Figure 2a that the backbone of the QueE−Mg^{2+} complex is basically equilibrated after 2 ns, which is earlier than that of QueE−Na^{+}. On the whole, a 20 ns MD simulation is sufficient for equilibrating the systems. The stabilized RMSD of QueE−Mg^{2+} is maintained at 1.3 Å, which is smaller than that of QueE−Na^{+} (1.8 Å). Figure 2b shows that the fluctuation of RMSFs of QueE−Na^{+} is similar to that of the QueE−Mg^{2+} complex, but some minor differences can also be found. For example, the RMSFs of residues 80−85 and 164 and the terminal of the QueE−Na^{+} protein are larger than that of QueE−Mg^{2+}. In addition, the fluctuations of residues 43, 65, 139, 144, 156, and 185 of the two systems are relatively large, indicating these residues display major conformational changes after MD simulations.

It should be noted that during the above MD simulations both Mg^{2+} and Na^{+} have been frozen on their crystal positions. It is a common strategy to prevent the collapse of the coordinate structures.[64,65] To check whether this scheme will influence the active-site structures of the two QueE−substrate complexes, we also performed 5 ns MD simulations without fixing the positions of Mg^{2+} and Na^{+}. The MD simulations

DOI: 10.1021/acscatal.5b00156
ACS Catal. 2015, 5, 3953−3965

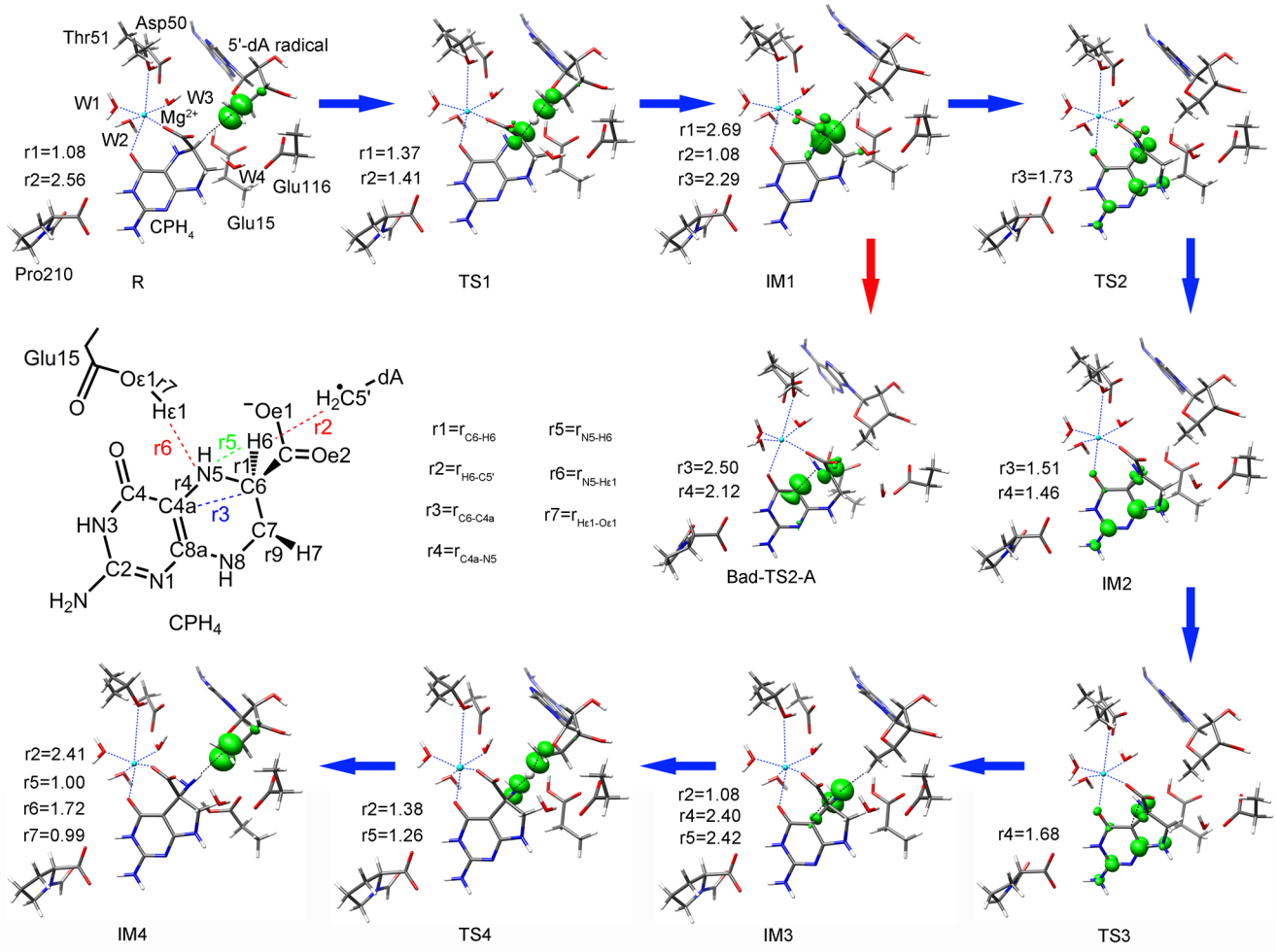

Figure 4. Optimized structures of the reactant, intermediates, and transition states of mutase reaction catalyzed by QueE–Mg^{2+} complex. The distances are given in angstroms. The isovalue of 0.01 au of the spin density was used.

showed that the coordination environments of the two metal ions have been obviously deviated from the crystal structures, especially for those of the QueE–Mg^{2+} complex, as shown in the Supporting Information (Figure S1). The main reason for causing the collapse of the coordinate structures can be attributed to the lack of effective force field parameters of metal–ligand interactions of Mg^{2+} and Na^{+}. Therefore, the last snapshots taken from 20 ns MD simulations, in which the positions of Mg^{2+} and Na^{+} were fixed, were used as the reactant structures to perform the subsequent QM/MM calculations.

The optimized active-site structures of QueE–Mg^{2+} and QueE–Na^{+} complexes are shown in Figure 3. By comparing the structures shown in Figures 1 and 3, one can see that the surrounding residues of the active sites were well kept after MD and QM/MM optimizations. A finding is that a noncrystal water molecule (W4) enters the reactive center and forms two hydrogen bonds with the carboxyl groups of CPH_4 and Glu116. This water (W4) may act as a mediator to promote the subsequent abstraction of the *pro-R* C7 proton. In both of the active sites of QueE–Mg^{2+} and QueE–Na^{+}, complex hydrogen bond networks are formed between CPH_4 and pocket residues. In the QueE–Mg^{2+} complex, in addition to coordinating with three water molecules and the hydroxyl group of Thr51, Mg^{2+} also directly interacts with the carboxyl and carbonyl groups of the substrate, forming a pseudo-octahedral core. In the complex of QueE–Na^{+}, the coordination of Na^{+} is similar to that of Mg^{2+}, but Na^{+} only ligates to the carboxyl group of CPH_4. It is the main difference of the active sites between the two complexes.

3.2. Calculated Reaction Mechanism of QueE–Mg^{2+} Complex. Mutase Reaction. In this work, the calculations started with the abstraction of a hydrogen atom from the substrate by the 5′-dA radical. Figure 4 shows the optimized structures of the reactant, transition states, and intermediates of the QM region. One can see that in the reactant R the C5′ atom of the 5′-dA radical locates at an ideal position to abstract the H6 atom of CPH_4 to initiate the catalytic cycle. From R to IM1, the distance (r2) between the C5′ and H6 atom changes from 2.56 to1.08 Å via 1.41 Å in TS1, and the distance of r1 (C6–H6) elongates from 1.08 to2.69 Å, suggesting that the H6 atom has been completely transferred to C5′ atom in IM1. Along with the abstraction of H6 atom, the unpaired spin density of the system is gradually transferred to the C6 atom, generating the C6-based radical intermediate (IM1). The spin density distribution on C5′ atom changes from 1.28 in R to −0.01 in IM1, and that of C6 atom changes accordingly from 0.00 to 0.88 (see Table S2). In IM1, the N5 atom and two oxygen atoms of carboxyl group delocalize 15% of spin density. In addition, the spin density of C4a increases from 0.00 in R to 0.05 in TS1 and finally delocalizes 9% of unpaired spin density of IM1, implying that the C4a atom can also stabilize the C6 radical by delocalizing the spin density.

DOI: 10.1021/acscatal.5b00156
ACS Catal. 2015, 5, 3953–3965

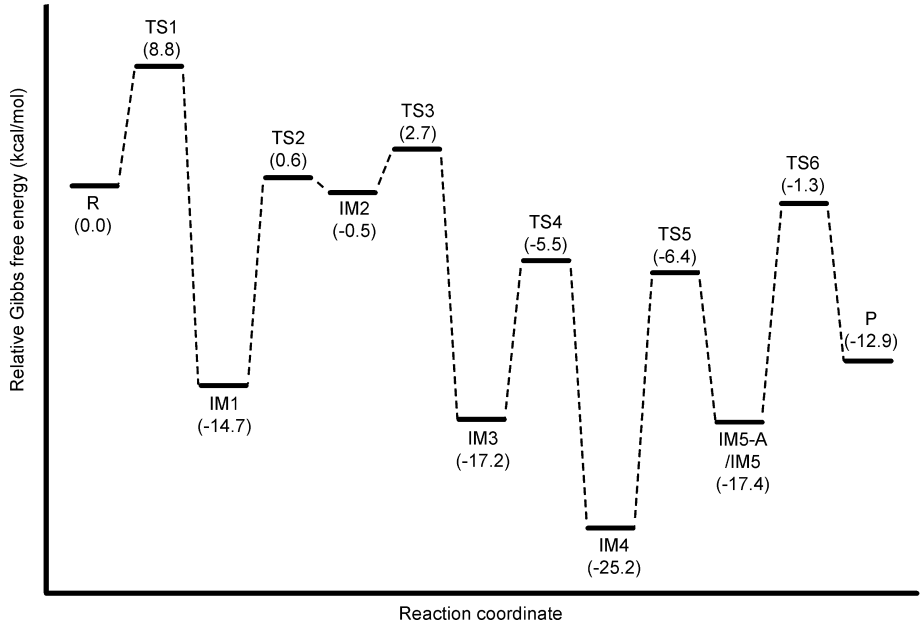

Figure 5. Relative Gibbs free energy profiles including the dispersion corrections for the reaction catalyzed by QueE-Mg^{2+}. The free energy of intermediate IM5 was set to the same value of IM5-A.

Table S3 shows the natural population atomic charges of some key atoms. A clear change in the H6-abstraction process can be found at the C6 atom. In R, the charge of C6 is −0.17 au; after the abstraction of H6, it changes to 0.15 au. As for N5 and C7 atoms, with the formation of the substrate radical (IM1), the charges of N5 and C7 atoms almost remain unchanged. It is understandable because the C6 atom bears the most spin density, while the adjacent N5 and C7 atoms only possess little spin density. Another interesting finding is the charge of Mg^{2+}. It always stays at 1.82, which implies that Mg^{2+} does not act as the Lewis acid during the H6-abstraction process.

The free energy barrier of the abstraction of H6 by the 5′-dA radical is calculated to be 8.8 kcal/mol, which means the C6-based radical intermediate (IM1) can be easily generated, as shown in Figure 5.

The next step is the radical-mediated ring-contraction step, which includes two elementary processes. The C6 radical of IM1 first attacks the C4a atom of the substrate to generate a bridged intermediate (IM2), which is followed by the cleavage of the C4a−N5 bond, yielding the nitrogen radical intermediate (IM3). From IM1 to IM2, the distance (r3) between C4a and C6 atom decreases from 2.29 Å in IM1 to 1.51 Å in IM2 via 1.73 Å in TS2. After formation of the C4a−C6 bond in IM2, the radical transfers from the C6 atom to other atoms such as C8a, C2, and C4. The Mulliken atomic spin densities of the related atoms are listed in Table S2 (Supporting Information). One can see that the unpaired spin density of C8a is only 0.34 in IM2, which means 66% of the radical has been delocalized to other atoms. As shown in Table S2 and Figure 4, the spin density of the C8a radical is obviously delocalized by the adjacent pyrimidine- and pyrrole-like rings in TS2 and IM2. In particular, the C2 atom delocalizes 25% of the spin density. The free energy barrier for the formation of IM2 is 15.3 kcal/mol (Figure 5). We also note that IM2 is an unstable intermediate, probably owing to the newly formed three-membered ring of N5−C6−C4a, which immediately rearranges to the nitrogen radical intermediate (IM3) to finish the ring contraction step by the cleavage of the C4a−N5 bond. This skeleton rearrangement corresponds to a very low free energy barrier of 3.2 kcal/mol. From IM2 to IM3, the tension of the three-membered ring no longer exists, and therefore, the nitrogen radical intermediate (IM3) is more stable than IM2. In IM3, the radical is mainly centered on the N5 atom with the spin density of 0.94 (Table S2), which is favorable for abstracting the hydrogen atom of C5′ to regenerate the 5′-dA radical. In this ring-contraction step from IM1 to IM3, the NPA charges of related atoms such as C4a, C6, and N5 show clear fluctuations, which change from −0.08, 0.15, and −0.69 au to −0.27, −0.06, and −0.49 au, respectively, as shown in Table S3.

As proposed in Scheme 3 and the previous studies,[29,30] in the ring contraction process, the C4a−N5 bond of IM1 may break directly and then undergo a *5-exo-trig* ring-closure step to finish the skeleton rearrangement. To further understand this ring-contraction process, the potential energy surface (PES) as a function of distances r3 (C4a−C6) and r4 (C4a−-N5) was also mapped out using the adiabatic mapping approach at the level of B3LYP/6-31G(d,p) for the QM region and the CHARMM22 force field for the MM region, as shown in Figure 6. The horizontal axis represents the cleavage of the C4a−N5 bond, and the vertical axis describes the formation of the C4a−C6 bond. The reaction coordinate of C4a−C6 ranges from 2.37 to1.50 Å with an increment of 0.03 Å, and that of C4a−N5 ranges from 1.45 to 2.40 Å with an increment of 0.05 Å. Thus, a total of 600 (30 × 20) structures were optimized for obtaining this PES. As shown in Figure 6, three low-energy regions can be recognized in the upper left, lower left, and lower right corners, respectively. The structure located at the upper left corner represents IM1, and the one at the lower right corner represents IM3. The low-energy region in the lower-left corner corresponds to the unstable intermediate IM2. The TS2 is situated in the area of r3 ≈ 1.73 Å and TS3 at the region of r4 ≈ 1.68 Å, which is in good agreement with the optimized transition-state structures shown in Figure 4. One can also see

DOI: 10.1021/acscatal.5b00156
ACS Catal. 2015, 5, 3953−3965

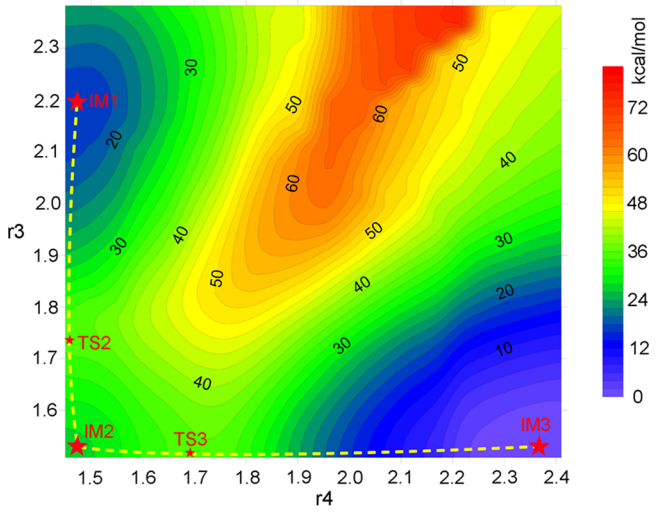

Figure 6. PES calculated at the B3LYP/6-31G(d,p) level using distances r3(C6−C4a) and r4(C4a−N5) as reaction coordinates.

from Figure 6 that the nitrogen radical is generated through the bridged intermediate rather than a ring-opening one. In addition, a structure with r4 of 2.12 Å and r3 of 2.50 Å was also found by using the scanning method, which can be named as Bad-TS2-A, as shown in Figure 4. Compared with TS2, the radical in Bad-TS2-A is mainly centered on the C4a and N5 atoms and is not delocalized by the adjacent atoms. Since Bad-TS2-A represents a higher energy structure, it is an impossible transition state.

After formation of IM3, the nitrogen radical abstracts the hydrogen atom of C5′ to regenerate the 5′-dA radical and forms the intermediate IM4 (initial product). The free energy barrier of this step is 11.7 kcal/mol. So far, the mutase reaction has been finished.

Deamination Reaction. In the deamination process, the amino group is eliminated from the substrate to form the 7-carboxy intermediate (IM5-A). The optimized structures of transition states, intermediates, and product are shown in Figure 7. One can see that, in the early stage of the deamination, the proton is transferred from the carboxyl group of residue Glu15 to the N5 atom to facilitate the elimination of the amino group. The elimination of ammonia molecule corresponds to a high free energy barrier of 18.8 kcal/mol. Since the protonated amino group bears one positive charge, it is necessary to analyze the changes of NPA charges in the related atoms. Table S3 shows that, along with the cleavage of C6−N5 bond, the charge of N5 atom exhibits a considerable variation, which changes from −0.89 au in IM4 to −1.01 in TS5. But the charge of Mg^{2+} also remains unchanged, implying that the Mg^{2+} does not act as a Lewis acid during the deamination process. In the literature,[29] it was proposed that the elimination of amino group may be facilitated by the residue Pro210 through its interaction with the exocyclic amino group of substrate. However, the charge of the exocyclic N atom is basically unchanged, suggesting the residue Pro210 may only have the function to stabilize the substrate. In IM5-A, the ligand molecules around the metal ion (Mg^{2+}) have been obviously disturbed owing to the interaction between NH_3 and Mg^{2+}. In particular, the formed ammonia molecule replaces the Thr51 to coordinate with the Mg^{2+}. According to the crystal structure of QueE in complex with Mg^{2+} and the product (PDB code: 4NJK),[29] the coordination between Thr51 and the metal ion was well kept during the catalytic reaction. Thus, the optimized structure of IM5-A may represent an unreasonable intermediate, and therefore, another possibility is considered;

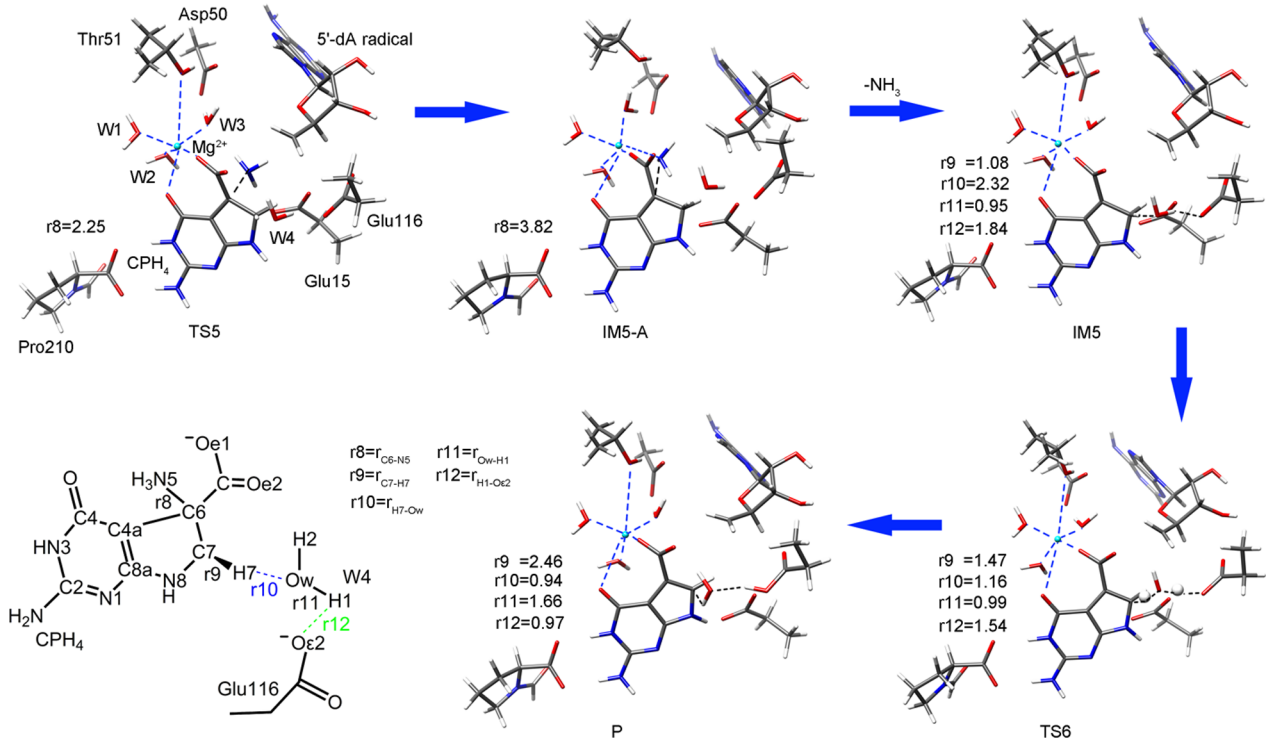

Figure 7. Optimized structures of the intermediates, transition states, and products of the deamination reaction catalyzed by the QueE−Mg^{2+} complex. The distances are given in angstroms.

DOI: 10.1021/acscatal.5b00156
ACS Catal. 2015, 5, 3953−3965

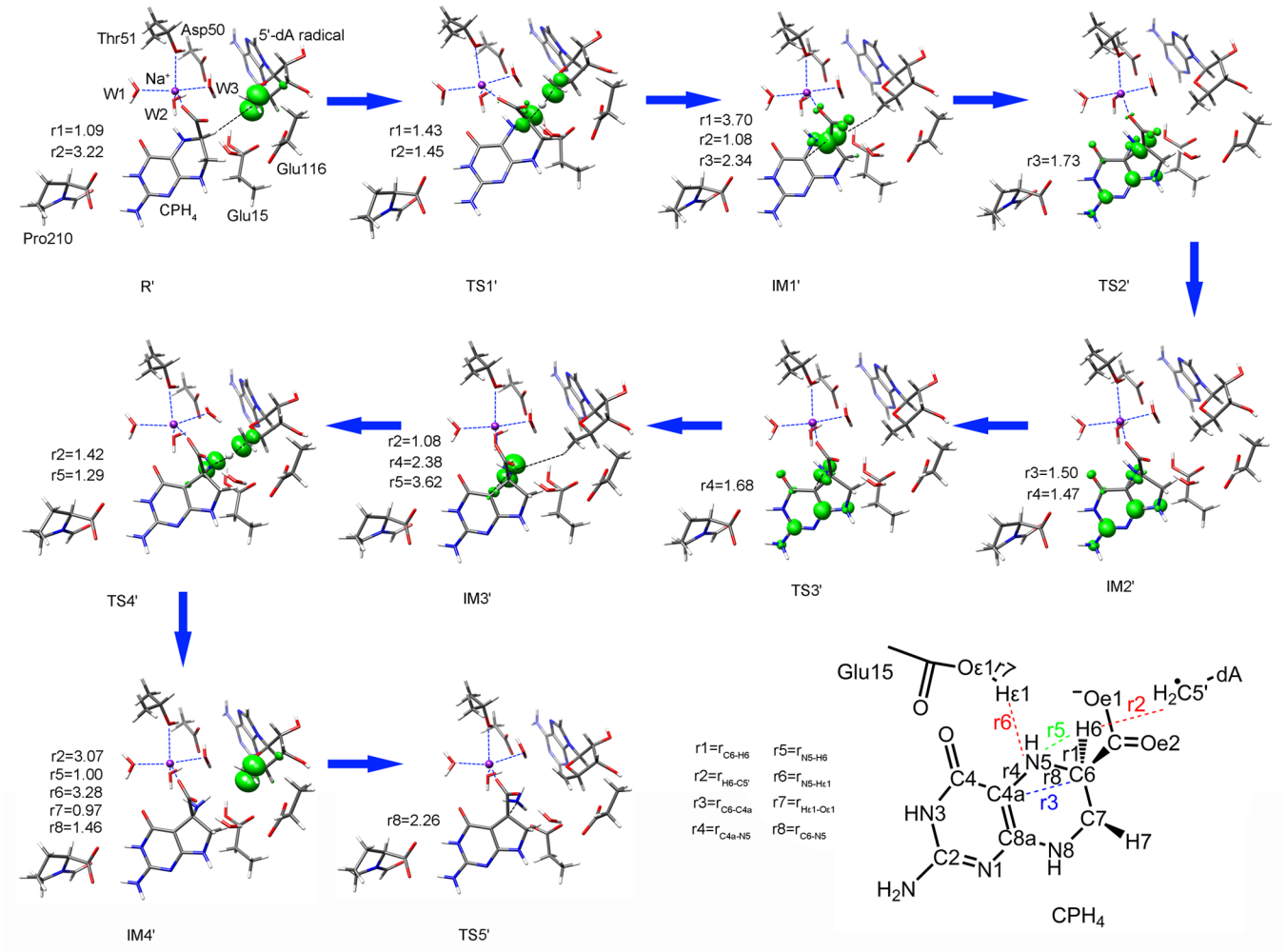

Figure 8. Optimized structures of the reactant, intermediates, and transition states of the reaction catalyzed by QueE in complex with Na^+. The distances are given in angstroms. The isovalue of 0.01 au of the spin density was used.

i.e., the generated ammonia molecule was removed from the active site to continue our QM/MM calculation. The optimized structure (IM5) is shown in Figure 7. It can be seen that, after removal of the ammonia molecule, the ligand environment around Mg^{2+} is well kept.

To form the final product CDG, the *pro-R* C7 proton must be deprotonated to aromatize the five-membered ring of the substrate. Abstraction of the *pro-R* C7 proton by the carboxyl group of Glu116 seems difficult because this proton is far away from the carboxyl group. Nevertheless, we note that a water molecule (W4) may act as a mediator to facilitate this proton-transfer process. The W4 molecule just locates between the *pro-R* C7 and residue Glu116, forming a perfect channel for proton transfer. As shown in IM5, a strong hydrogen bond is formed between the H1 atom of W4 and Oε2 atom of Glu116 with a distance of 1.84 Å (r12). In addition, the H7 atom of the substrate orients to the Ow of W4 and the distance is 2.32 Å (r10). According to the results of our calculations, the proton transfer of this step proceeds in a concerted but asynchronous manner. With the H7 proton transferring to the Ow atom of W4, the H1 atom is gradually abstracted by residue Glu116. The corresponding distance of r10 decreases from 2.32 Å in IM5 to 1.16 Å in TS6 and further decreases to 0.94 Å in P. Simultaneously, the distance of r11 increases from 0.99 Å in TS6 to 1.66 Å in P. In the optimized structure of product P, a strong hydrogen bond is formed between the water molecule (W4) and Glu116. The corresponding free energy barrier of this step is 16.1 kcal/mol.

For comparison, we also calculated the deprotonation process of the *pro-R* C7 proton without the assistance of mediator water molecule (W4). During the calculations, the water molecule was removed from the reaction center of IM5. The calculated results are shown in Figures S2 and S3 of the Supporting Information. We can see that the energy barrier at B3LYP/6-311++G(3df,3pd) level increases from 15.3 to 21.6 kcal/mol.

In summary, the elimination process of ammonia is calculated to be the rate-limiting step with the free energy barrier of 18.8 kcal/mol, which is a little bit smaller than the estimated value (20.9 kcal/mol) from the measured k_{cat} by the classical transition-state theory. In the assays of QueE−Mg^{2+} from *B. multivorans*, the final k_{cat} value is 0.19 ± 0.06 min^{-1}.[29] Although the DFT method usually underestimates the energy barrier, we should realize that the calculated result (18.8 kcal/mol) was only derived from one snapshot of the MD simulations; therefore, it is not conclusive considering the sampling of our QM/MM calculations. As for the rate-limiting step of the whole catalytic reaction, the elimination process of ammonia is calculated to be rate limiting, but we also note that the final aromatization corresponds to a free energy barrier of

DOI: 10.1021/acscatal.5b00156
ACS Catal. 2015, 5, 3953−3965

16.1 kcal/mol under the assistance of a mediated water molecule. Without this water, the energy barrier increases to 21.6 kcal/mol. Therefore, it is also a possible rate-limiting step. In addition, based on the calculated free energy profile, an intermediate (IM4) has the lowest relative energy, which may be probed by future experiments.

3.3. Influence of Metal Ions and the Electrostatic Effect of Environment. As described above, the active site of the QueE−Na^+ complex is similar to that of the QueE−-Mg^{2+}. The main difference between the two systems is that Na^+ only coordinates to the carboxyl group of the substrate, while Mg^{2+} not only coordinates to the carboxyl group but also ligates to the carbonyl group of the substrate (Figures 1 and 3).[29] Although the environmental difference around the active sites is minor, the enzyme displays different activity. To investigate how the metal ions influence the enzymatic reaction, the mutase and deamination reactions catalyzed by QueE in complex with Na^+ were also calculated by using the same strategy. The optimized structures of reactant, transition states, and intermediates are shown in Figure 8. The energy profiles of the catalytic reactions of the QueE−Na^+ and QueE−Mg^{2+} complexs are compared in Figure 9.

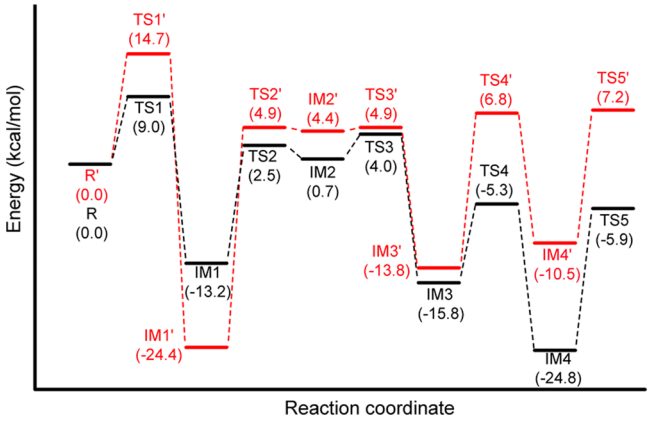

Figure 9. Energy profiles including the dispersion corrections along the reactions catalyzed by QueE−Mg^{2+} (black) and QueE−Na^+ (red) at the B3LYP/6-311++G(3df,3pd) level. Both energies of the two reactants were set to zero.

As shown in Figures 8 and 9, the catalytic reaction pathway of the QueE−Na^+ complex is not changed compared with that of the QueE−Mg^{2+}, but their energy profiles show little difference. The energy barriers of the first, second, and fourth steps show clearly increase for QueE−Na^+ complex, which will be discussed in detail in the next contexts.

For the first step, the energy barrier of the QueE−Na^+ complex increases by 5.7 kcal/mol compared to that of QueE−Mg^{2+}. It can be attributed to the different interactions of Mg^{2+} and Na^+ with the substrate. In the QueE−Na^+ complex, Na^+ only coordinates to the carboxyl group of the substrate, leading to the substrate molecule being far away from 5′-dA radical. As a result, the distance (r2) between the H6 atom and the C5′ radical increases from 2.56 Å in QueE−Mg^{2+} to 3.22 Å in QueE−Na^+, which is supposed to be the main reason for the increase of the energy barrier of the H6-abstracting step. In addition, after formation of the C6 radical (IM1′), the distance (r1) between the C6 and H6 atoms in QueE−Na^+ system is larger than that in the QueE−Mg^{2+} system, and the resulted intermediate IM1′ is more stable. By comparing the atomic spin densities and NPA charges of QueE−Na^+ system (Tables S4 and S5) with those of the QueE−Mg^{2+} system (Tables S2 and S3), we can see that the two systems display similar changing characteristics. For example, with the formation of C6 radical, the spin density distribution on the C5′ atom changes from 1.28 and 1.14 in R and R′ to −0.01 and 0.00 in IM1 and IM1′ and that of C6 atom changes from 0.00 and −0.04 to 0.88 and 0.91, respectively; the NPA charge on C6 atom changes from −0.17 and −0.17 au in R and R′ to 0.15 and 0.10 au in IM1 and IM1′, respectively.

In the step of C4a−C6 bond formation, the energy barriers for the two systems are quite different. It is 15.7 kcal/mol for the QueE−Mg^{2+} system, while it raises to 29.3 kcal/mol in the QueE−Na^+ system. We may attribute it to the different changes of NPA charges of the ring atoms of the substrate. For example, the charge of C6 atom changes 0.20 au from IM1 to TS2, whereas it only changes 0.03 au from IM1′ to TS2′. In the fourth step to regenerate the 5′-dA radical, the energy barrier of the QueE−Na^+ system increases by 10.1 kcal/mol. This increase can be attributed to the larger distance (r5) between the H6 atom and the N5 radical in IM3′. r5 is 3.62 Å in IM3′, but it is only 2.42 Å in IM3. We also note that the relative energies of IM4′ and TS5′ are higher than those of IM4 and TS5.

Another interesting finding is the charges of Na^+ and Mg^{2+} ions. As shown in Tables S3 and S5, during the catalytic reaction, both of the charges of Na^+ and Mg^{2+} remain unchanged. Thus, both of them do not act as Lewis acids during the catalytic reaction but influence the spatial orientations of the substrate by differently interacting with it. As previously mentioned, in the QueE−Mg^{2+} complex, Mg^{2+} coordinates with both the carbonyl and carboxyl groups of the substrate, but in the QueE−Na^+ complex Na^+ only coordinates with the carboxyl group of the substrate. The distances between the two metal ions and the oxygen atoms of carbonyl and carboxyl groups of substrate are shown in Figure 10. One can

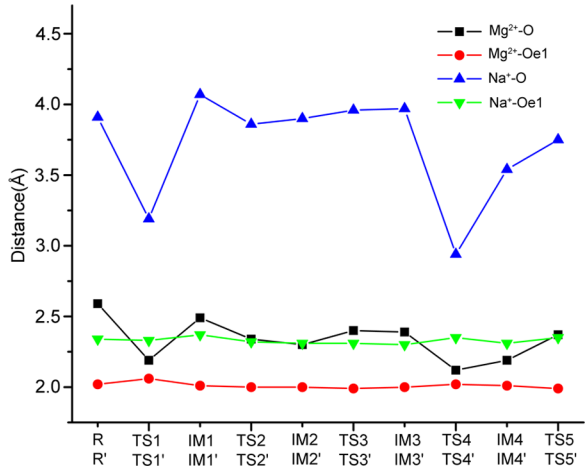

Figure 10. Distances between Mg^{2+} (Na^+) and the ligated atoms of Mg^{2+} (Na^+)-coordinated molecules.

see that the distances between the Na^+ and oxygen atom of carbonyl group (Na−O) are always larger than 3.0 Å, implying the interaction between the Na^+ and carbonyl group is very weak, but the distances between the Mg^{2+} and the oxygen atom of carbonyl group (Mg^{2+}−O) show obvious fluctuation during the catalytic reaction, such as in the steps of R → IM1, IM1 →

DOI: 10.1021/acscatal.5b00156
ACS Catal. 2015, 5, 3953−3965

IM2, IM3 → IM4, and IM4 → TS5. Besides, the distances (Mg^{2+}−Oe1 and Na^{+}−Oe1) between the metal ions and the carboxyl group are almost unchanged. In addition, the distance of Mg−Oe1 is always shorter than that of the Na^{+}−Oe1.These results indicate that the interaction between Mg^{2+} and the carboxyl group are stronger than that of Na^{+}.

In the QueE−Mg^{2+} complex, the ammonia elimination process is suggested to be the rate-limiting step with the free energy barrier of 18.8 kcal/mol and energy barrier of 18.9 kcal/mol (Figures 5 and 9). In the QueE−Na^{+} complex, however, the rate-limiting step changes. The step of C6−C4a bond formation is calculated to be rate limiting with an energy barrier of 29.3 kcal/mol.

The different features of the energy profiles of QueE−Mg^{2+} and QueE−Na^{+} systems seem to be mainly caused by the different coordination of Mg^{2+} and Na^{+} with the substrate, which causes some key distance differences. For example, in the first step, the distances (r2) between the H6 atom and the C5′ radical of QueE−$Mg^{2+}$and QueE−Na^{+} systems are 2.56 and 3.22 Å, corresponding to the energy barriers of 9.0 and 14.7 kcal/mol, respectively.

For comparison, we also studied how the initial structure influences the energy profile. For the QueE−Na^{+} complex, a starting structure (R″) was further taken from a snapshot of MD trajectory at 19 ns, and the corresponding QM/MM calculations were performed. The optimized structures of the reactant, intermediates, and transition states for the mutase and deamination reactions at the B3LYP/6-31G(d,p) level are shown in Figure S4, and the energy profile at the B3LYP/6-31++G(d,p) level in comparison with the results of the snapshot taken at 20 ns is displayed in Figure S5. One can see that the two calculated energy profiles are very similar, and the energy barriers of the rate-limiting step from the two snapshots at 19 and 20 ns are 27.4 and 28.0 kcal/mol, respectively. Therefore, the initial structures only have a minor influence on the energy barrier of the rate-limiting step.

To evaluate the influence of electrostatic effect of MM subsystems on the QM region energies, the energies of $E_{QM+ptch}$ are derived from the QM/MM calculations and are compared with the energies of E_{QM}. The $E_{QM+ptch}$ characterizes the QM region energy calculated in the field of MM point charges, and the E_{QM} describes the QM region energy calculated without the point charges at the same basis set by using Gaussian03 package. Thus, the differences between the E_{QM} and $E_{QM+ptch}$ represent the electrostatic effect of environments. The E_{QM} and $E_{QM+ptch}$ of QueE in complex with Mg^{2+} and Na^{+} are shown in Figure 11. As shown in Figure11, the influence of electrostatic effect of surroundings on the QM region of QueE−Mg^{2+} is great in TS1, IM2, TS4, and TS5, and the QM region energies of the QueE−Na^{+} complex suffer a greater influence by electrostatic effects than those of the QueE−Mg^{2+}complex.

We also investigated the structural change of QueE in complex with Mg^{2+} at the absence of substrate. On the basis of the optimized structure of P, the product CDG was removed from the active site, and the resulting system was performed for an additional 8 ns MD simulation. The obtained RMSD is shown in Figure S6, and the structure of the active site after MD simulation is shown in Figure S7. One can see that the environment around the active site is only slightly changed. However, we note that the side chain of residue Gln13 undergoes a rotation around the Cβ−Cγ bond, by which the dihedral angle ($\varphi_{C\alpha-C\beta-C\gamma-C\delta}$) changes by 102.66° compared to the QueE in complex with the substrate (Figure 3a). Therefore,

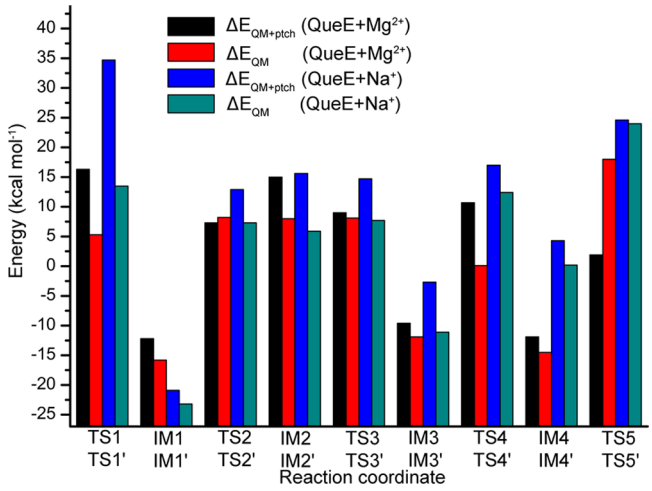

Figure 11. Relative energies of QM region calculated at the field of MM point charges ($\Delta E_{QM+ptch}$) and QM region energies without point charges (ΔE_{QM}) for QueE−Mg^{2+} and QueE−Na^{+} complexes. All the energies are calculated at the B3LYP/6-31++G(d,p) level. The energies of the two reactants (R and R′) were set to zero.

the residue Gln13 may have the function to control the release of the product CDG. In addition, the substrate-binding pocket is occupied by several water molecules, and two of them replace the carboxyl and carbonyl groups of CPH_4 to coordinate with Mg^{2+}. A hydrogen bond is formed between the residues Glu15 and Glu116, which may facilitate the proton transfer from Glu116 to Glu15 to reconstitute the reactive state of QueE.

In summary, on the basis of our calculation results, the catalytic mechanism of QueE has been delineated more clearly. In the previous study by Dowling et al.,[29] it was proposed that, after the formation substrate radical, a number of routes are possible to generate the five-membered pyrrole ring. The reaction may undergo an azocyclopropyl radical intermediate or proceed through complex opening−closing steps. Our calculations give the answer that the key ring contraction step involves a bridged intermediate rather than a ring-opening one. In addition, the present work provides the details of how the nitrogen radical abstracts the hydrogen atom of C5′ to regenerate the 5′-dA radical and how the pro-R C7 proton is deprotonated by the nearby residue to aromatize the five-membered ring of the substrate. This information cannot be derived from experiments alone.

We should note that the SAM radical enzymes belong to a superfamily whose members have been estimated to surpass 50000.[21] A common feature of these enzymes is that all of them catalyze the reductive cleavage of AdoMet (SAM) to generate the highly reactive and unstable oxidant 5′-deoxyadenosyl radical ($dA^{\bullet}$) to initiate the chemistry in the active sites. The SAM radical enzymes differ from the ordinary enzymes in that the specific reactions catalyzed by SAM radical enzymes show amazingly diversity, which include carbon methylation, sulfur insertion, oxidation, methylthiolation, and complex carbon skeleton rearrangements. We can envision that these catalytic reactions follow different mechanism except they use the same [4Fe−4S] cluster and SAM. Owing to the limitation of crystal structures, the knowledge about the reaction mechanism is still very hazy, and the theoretical studies for understanding the chemistry of SAM enzymes are highly deserved.

Although QueE belongs to the radical *S*-adenosylmethionine (SAM) enzyme superfamily, it displays different features

DOI: 10.1021/acscatal.5b00156
ACS Catal. 2015, 5, 3953−3965

compared to the other radical SAM enzymes. As described in the Introduction, the typical SAM enzymes have the conserved motif of $CX_3CX\Phi C$, while QueE from *B. multivorans* contains the unique motif of $CX_{14}CX\Phi C$. Besides, QueE shows a clear dependence on Mg^{2+} ion. On the basis of our calculations, the role of metal ions has been illuminated. Natural population analysis indicates that, during the catalytic reaction, the metal ions do not act as Lewis acids. They presumably play a role in fixing the substrate in its reactive conformation. On the basis of the crystal structures, Dowling et al. suggested that Na^+ and Mn^{2+} cannot substitute for Mg^{2+} because they interact differently with the substrate.[29] Our calculations also confirm this point; i.e., it is the different coordination of Mg^{2+} and Na^+ with the substrate that leads to the different activities of QueE−Mg^{2+} and QueE−Na^+ complexes.

As for the QueE from *B. subtilis*,[30] its crystal structure has not determined yet. Therefore, we cannot give detailed comparison of the QueE from *B. subtilis* and *B. multivorans*, but both of the enzymes catalyze the conversion of 6-carboxy-5,6,7,8-tetrahydropterin (CPH_4) to CDG, and they should have similar active structures to accommodate the substrate and similar residues to finish the chemical reaction. For example, the H6 atom of CPH_4 (substrate) should locate in an ideal position for its abstraction by the 5′-dA radical, and a nearby protonated residue is required to protonate the NH_2 of the substrate. Another deprotonated residue is also necessary to abstract the pro-R C7 proton to complete the aromatization of the substrate. Although experiments showed that QueE's from *B. multivorans* and *B. subtilis* differ markedly in terms of structures,[29] for example, QueE from *B. subtilis* contains the traditional $CX_3CX\Phi C$ motif, while QueE from *B. multivorans* has the modified $CX_{14}CX\Phi C$ motif, they must share some common features in their active centers.

4. CONCLUSION

The detailed catalytic mechanism of QueE in complex with Mg^{2+} and Na^+ has been investigated at an atomistic level by using the QM/MM method. The complex and heterocyclic rearrangement of the carbon skeleton follows a radical-mediated mechanism. The 5′-dA radical first abstracts a hydrogen atom from C6 of the substrate to initiate the catalytic reaction. The ring-contraction step involves a bridged intermediate but not a ring-opening one. On the basis of the results of our calculations, we speculate that the generated ammonia molecule may immediately diffuse to the solvent upon its formation. The abstraction of *pro-R* C7 proton by the residue Glu116 to aromatize the product may be mediated by an active-site water molecule. On the basis of our calculations, the elimination of ammonia molecule is calculated to be rate limiting for the QueE−Mg^{2+} system with a free energy barrier of 18.8 kcal/mol, which agrees basically with the estimated value (20.9 kcal/mol) from the measured k_{cat}. For QueE−Na^+ complex, the formation of the bridged intermediate corresponds to a higher energy barrier of 29.3 kcal/mol, suggesting the formation of C4a−C6 bond is the rate-limiting step. According to our calculations, Mg^{2+} and Na^+ ions do not act as Lewis acids but mainly play a role in fixing the conformation of the substrate. Our results may provide useful information for further understanding the catalytic mechanism of QueE.

■ ASSOCIATED CONTENT

Supporting Information

The Supporting Information is available free of charge on the ACS Publications website at DOI: 10.1021/acscatal.5b00156.

Calculated relative entropy effects and empirical dispersion corrections for QueE−Mg^{2+} complex, Mulliken atomic spin densities and NPA charges of selected atoms for QueE-Mg^{2+} and Na^+ complexes, active-site structures of QueE−Mg^{2+} and QueE−Na^+ complexes taken from a 5 ns MD simulation without fixing the positions of Mg^{2+} and Na^+, optimized structures and energy profiles of the *pro-R* C7 proton direct abstraction process catalyzed by QueE−Mg^{2+}, optimized structures of pathway R″ → TS5″ catalyzed by the QueE−Na^+ complex, energy profile along the reaction catalyzed by QueE−Na^+ complex by using R′ and R″ as reactants, RMSDs and active-site structure of QueE in complex with Mg^{2+} in the absence of substrate taken from a 8 ns MD simulation (PDF)

■ AUTHOR INFORMATION

Corresponding Author

*Tel: +86 531 883 655 76. Fax: +86 531 885 644 64. E-mail: yongjunliu_1@sdu.edu.cn.

Notes

The authors declare no competing financial interest.

■ ACKNOWLEDGMENTS

This work was supported by the Natural Science Foundation of China (21173129, 21373125) and the Taishan Scholars Climbing Program of Shandong Province.

■ REFERENCES

(1) Nishimura, H.; Katagiri, K.; Sato, K.; Mayama, M.; Shimaoka, N. *J. Antibiot.* **1956**, *9*, 60−62.
(2) Suhadolnik, R. J. Pyrrolopyrimidine nucleosides. In *Nucleoside Antibiotics*; Wiley-Interscinece: New York, 1970; p 298.
(3) Wu, R. T.; Okabe, T.; Namikoshi, M.; Okuda, S.; Nishimura, T.; Tanaka, N. *J. Antibiot.* **1982**, *35*, 279−284.
(4) McCarty, R. M.; Bandarian, V. *Bioorg. Chem.* **2012**, *43*, 15−25.
(5) Kasai, H.; Ohashi, Z.; Harada, F.; Nishimura, S.; Oppenheimer, N. J.; Crain, P. F.; Liehr, J. G.; von Minden, D. L.; McCloskey, J. A. *Biochemistry* **1975**, *14*, 4198−4208.
(6) Gregson, J. M.; Crain, P. F.; Edmonds, C. G.; Gupta, R.; Hashizume, T.; Phillipson, D. W.; McCloskey, J. A. *J. Biol. Chem.* **1993**, *268*, 10076−10086.
(7) Harada, F.; Nishimura, S. *Biochemistry* **1972**, *11*, 301−308.
(8) Kasai, H.; Nakanishi, K.; Macfarlane, R. D.; Torgerson, D. F.; Ohashi, Z.; McCloskey, J. A.; Gross, H. J.; Nishimura, S. *J. Am. Chem. Soc.* **1976**, *98*, 5044−5046.
(9) White, B. N.; Tener, G. M.; Holden, J.; Suzuki, D. T. *J. Mol. Biol.* **1973**, *74*, 635−651.
(10) Edmonds, C. G.; Crain, P. F.; Gupta, R.; Hashizume, T.; Hocart, C. H.; Kowalak, J. A.; Pomerantz, S. C.; Stetter, K. O.; McCloskey, J. A. *J. Bacteriol.* **1991**, *173*, 3138−3148.
(11) McCarty, R. M.; Somogyi, Á.; Lin, G.; Jacobsen, N. E.; Bandarian, V. *Biochemistry* **2009**, *48*, 3847−3852.
(12) Bandarian, V. *Biochim. Biophys. Acta, Proteins Proteomics* **2012**, *1824*, 1245−1253.
(13) McCarty, R. M.; Bandarian, V. *Chem. Biol.* **2008**, *15*, 790−798.
(14) Bracher, A.; Eisenreich, W.; Schramek, N.; Ritz, H.; Götze, E.; Herrmann, A.; Gütlich, M.; Bacher, A. *J. Biol. Chem.* **1998**, *273*, 28132−28141.

DOI: 10.1021/acscatal.5b00156
ACS Catal. 2015, 5, 3953−3965

(15) McCarty, R. M.; Somogyi, A.; Bandarian, V. *Biochemistry* **2009**, *48*, 2301−2303.
(16) Fontecave, M.; Mulliez, E.; Ollagnier-de-Choudens, S. *Curr. Opin. Chem. Biol.* **2001**, *5*, 506−511.
(17) Sofia, H. J.; Chen, G.; Hetzler, B. G.; Reyes-Spindola, J. F.; Miller, N. E. *Nucleic Acids Res.* **2001**, *29*, 1097−1106.
(18) Dowling, D. P.; Vey, J. L.; Croft, A. K.; Drennan, C. L. *Biochim. Biophys. Acta, Proteins Proteomics* **2012**, *1824*, 1178−1195.
(19) Vey, J. L.; Drennan, C. L. *Chem. Rev.* **2011**, *111*, 2487−2506.
(20) Wang, J.; Woldring, R. P.; Román-Meléndez, G. D.; McClain, A. M.; Alzua, B. R.; Marsh, E. N. G. *ACS Chem. Biol.* **2014**, *9*, 1929−1938.
(21) Broderick, J. B.; Duffus, B. R.; Duschene, K. S.; Shepard, E. M. *Chem. Rev.* **2014**, *114*, 4229−4317.
(22) Atta, M.; Arragain, S.; Fontecave, M.; Mulliez, E.; Hunt, J. F.; Luff, J. D.; Forouhar, F. *Biochim. Biophys. Acta, Proteins Proteomics* **2012**, *1824*, 1223−1230.
(23) Krebs, C.; Broderick, W. E.; Henshaw, T. F.; Broderick, J. B.; Huynh, B. H. *J. Am. Chem. Soc.* **2002**, *124*, 912−913.
(24) Zhang, Y.; Zhu, X.; Torelli, A. T.; Lee, M.; Dzikovski, B.; Koralewski, R. M.; Wang, E.; Freed, J.; Krebs, C.; Ealick, S. E.; Lin, H. *Nature* **2010**, *465*, 891−896.
(25) Walsby, C. J.; Ortillo, D.; Broderick, W. E.; Broderick, J. B.; Hoffman, B. M. *J. Am. Chem. Soc.* **2002**, *124*, 11270−11271.
(26) Walsby, C. J.; Ortillo, D.; Yang, J.; Nnyepi, M. R.; Broderick, W. E.; Hoffman, B. M.; Broderick, J. B. *Inorg. Chem.* **2005**, *44*, 727−741.
(27) Zhang, Q.; Liu, W. *J. Biol. Chem.* **2011**, *286*, 30245−30252.
(28) Arragain, S.; Garcia-Serres, R.; Blondin, G.; Douki, T.; Clemancey, M.; Latour, J. M.; Forouhar, F.; Neely, H.; Montelione, G. T.; Hunt, J. F.; Mulliez, E.; Fontecave, M.; Atta, M. *J. Biol. Chem.* **2010**, *285*, 5792−5801.
(29) Dowling, D. P.; Bruender, N. A.; Young, A. P.; McCarty, R. M.; Bandarian, V.; Drennan, C. L. *Nat. Chem. Biol.* **2013**, *10*, 106−112.
(30) McCarty, R. M.; Krebs, C.; Bandarian, V. *Biochemistry* **2013**, *52*, 188−198.
(31) Baldwin, J. E. *J. Chem. Soc., Chem. Commun.* **1976**, 734−736.
(32) Frey, P. A.; Reed, G. H. *Biochim. Biophys. Acta, Proteins Proteomics* **2011**, *1814*, 1548−1557.
(33) Warshel, A.; Karplus, M. *J. Am. Chem. Soc.* **1972**, *94*, 5612−5625.
(34) Warshel, A.; Levitt, M. *J. Mol. Biol.* **1976**, *103*, 227−249.
(35) Grigorenko, B. L.; Khrenova, M. G.; Nilov, D. K.; Nemukhin, A. V.; Švedas, V. K. *ACS Catal.* **2014**, *4*, 2521−2529.
(36) Saura, P.; Suardíaz, R.; Masgrau, L.; Lluch, J. M.; González-Lafont, À. *ACS Catal.* **2014**, *4*, 4351−4363.
(37) Wu, R. B.; Cao, Z. X. *J. Comput. Chem.* **2008**, *29*, 350−357.
(38) Elsässer, B.; Schoenen, I.; Fels, G. *ACS Catal.* **2013**, *3*, 1397−1405.
(39) Wu, E. L.; Wong, K.; Zhang, X.; Han, K. L.; Gao, J. L. *J. Phys. Chem. B* **2009**, *113*, 2477−2485.
(40) Kamachi, T.; Kouno, T.; Doitomi, K.; Yoshizawa, K. *J. Inorg. Biochem.* **2011**, *105*, 850−857.
(41) Rommel, J. B.; Kästner, J. *J. Am. Chem. Soc.* **2011**, *133*, 10195−10203.
(42) Zhu, W.; Liu, Y.; Zhang, R. *Theor. Chem. Acc.* **2013**, *132*, 1385−1392.
(43) Li, H.; Robertson, A. D.; Jensen, J. H. *Proteins: Struct., Funct., Genet.* **2005**, *61*, 704−721.
(44) Bas, D. C.; Rogers, D. M.; Jensen, J. H. *Proteins: Struct., Funct., Genet.* **2008**, *73*, 765−783.
(45) Olsson, M. H. M.; Søndergaard, C. R.; Rostkowski, M.; Jensen, J. H. *J. Chem. Theory Comput.* **2011**, *7*, 525−537.
(46) Søndergaard, C. R.; Olsson, M. H. M.; Rostkowski, M.; Jensen, J. H. *J. Chem. Theory Comput.* **2011**, *7*, 2284−2295.
(47) Brooks, B. R.; Bruccoleri, R. E.; Olafson, B. D.; States, D. J.; Swaminathan, S.; Karplus, M. *J. Comput. Chem.* **1983**, *4*, 187−217.
(48) Jorgensen, W. L.; Chandrasekhar, J.; Madura, J. D.; Impey, R. W.; Klein, M. L. *J. Chem. Phys.* **1983**, *79*, 926−935.
(49) Chen, J. H.; Im, W. P.; Brooks, C. L. *J. Am. Chem. Soc.* **2006**, *128*, 3728−3736.
(50) MacKerell, A. D., Jr.; Bashford, D.; Bellott, M.; Dunbrack, R. L., Jr.; Evanseck, J. D.; Field, M. J.; Fischer, S.; Gao, J.; Guo, H.; Ha, S.; Joseph-McCarthy, D.; Kuchnir, L.; Kuczera, K.; Lau, F. T. K.; Mattos, C.; Michnick, S.; Ngo, T.; Nguyen, D. T.; Prodhom, B.; Reiher, W. E., III; Roux, B.; Schlenkrich, M.; Smith, J. C.; Stote, R.; Straub, J.; Watanabe, M.; Wiórkiewicz-Kuczera, J.; Yin, D.; Karplus, M. *J. Phys. Chem. B* **1998**, *102*, 3586−3616.
(51) Lee, C.; Yang, W.; Parr, R. G. *Phys. Rev. B: Condens. Matter Mater. Phys.* **1988**, *37*, 785−789.
(52) Becke, A. D. *J. Chem. Phys.* **1993**, *98*, 5648−5652.
(53) Ahlrichs, R.; Bar, M.; Haser, M.; Horn, H.; Kolmel, C. *Chem. Phys. Lett.* **1989**, *162*, 165−169.
(54) Smith, W.; Forester, T. R. *J. Mol. Graphics* **1996**, *14*, 136−141.
(55) Sherwood, P.; de Vries, A. H.; Guest, M. F.; Schreckenbach, G.; Catlow, C. R. A.; French, S. A.; Sokol, A. A.; Bromley, S. T.; Thiel, W.; Turner, A. J.; Billeter, S.; Terstegen, F.; Thiel, S.; Kendrick, J.; Rogers, S. C.; Casci, J.; Watson, M.; King, F.; Karlsen, E.; Sjøvoll, M.; Fahmi, A.; Schäfer, A.; Lennartz, C. *J. Mol. Struct.: THEOCHEM* **2003**, *632*, 1−28.
(56) de Vries, A. H.; Sherwood, P.; Collins, S. J.; Rigby, A. M.; Rigutto, M.; Kramer, G. J. *J. Phys. Chem. B* **1999**, *103*, 6133−6141.
(57) Bakowies, D.; Thiel, W. *J. Phys. Chem.* **1996**, *100*, 10580−10594.
(58) Billeter, S. R.; Turner, A. J.; Thiel, W. *Phys. Chem. Chem. Phys.* **2000**, *2*, 2177−2186.
(59) Nocedal, J. *Math. Comput.* **1980**, *35*, 773−782.
(60) Liu, D. C.; Nocedal, J. *Math. Prog.* **1989**, *45*, 503−528.
(61) Banerjee, A.; Adams, N.; Simons, J.; Shepard, R. *J. Phys. Chem.* **1985**, *89*, 52−57.
(62) Grimme, S.; Antony, J.; Ehrlich, S.; Krieg, H. *J. Chem. Phys.* **2010**, *132*, 154104−154123.
(63) Frisch, M. J.; Trucks, G. W.; Schlegel, H. B.; Scuseria, G. E.; Robb, M. A.; Cheeseman, J. R.; Montgomery, J. A., Jr.; Vreven, T.; Kudin, K. N.; Burant, J. C.; Millam, J. M.; Iyengar, S. S.; Tomasi, J.; Barone, V.; Mennucci, B.; Cossi, M.; Scalmani, G.; Rega, N.; Petersson, G. A.; Nakatsuji, H.; Hada, M.; Ehara, M.; Toyota, K.; Fukuda, R.; Hasegawa, J.; Ishida, M.; Nakajima, T.; Honda, Y.; Kitao, O.; Nakai, H.; Klene, M.; Li, X.; Knox, J. E.; Hratchian, H. P.; Cross, J. B.; Bakken, V.; Adamo, C.; Jaramillo, J.; Gomperts, R.; Stratmann, R. E.; Yazyev, O.; Austin, A. J.; Cammi, R.; Pomelli, C.; Ochterski, J. W.; Ayala, P. Y.; Morokuma, K.; Voth, G. A.; Salvador, P.; Dannenberg, J. J.; Zakrzewski, V. G.; Dapprich, S.; Daniels, A. D.; Strain, M. C.; Farkas, O.; Malick, D. K.; Rabuck, A. D.; Raghavachari, K.; Foresman, J. B.; Ortiz, J. V.; Cui, Q.; Baboul, A. G.; Clifford, S.; Cioslowski, J.; Stefanov, B. B.; Liu, G.; Liashenko, A.; Piskorz, P.; Komaromi, I.; Martin, R. L.; Fox, D. J.; Keith, T.; Al-Laham, M. A.; Peng, C. Y.; Nanayakkara, A.; Challacombe, M.; Gill, P. M. W.; Johnson, B.; Chen, W.; Wong, M. W.; Gonzalez, C.; Pople, J. A. *GAUSSIAN 03 (Revision D.01)*, Gaussian, Inc., Wallingford, CT, 2004.
(64) Wang, B. J.; Usharani, D.; Li, C. S.; Shaik, S. *J. Am. Chem. Soc.* **2014**, *136*, 13895−13901.
(65) Wu, R. B.; Wang, S. L.; Zhou, N. J.; Cao, Z. X.; Zhang, Y. K. *J. Am. Chem. Soc.* **2010**, *132*, 9471−9479.

DOI: 10.1021/acscatal.5b00156
ACS Catal. 2015, 5, 3953−3965